

Realizing the Frenkel-Kontorova model with Rydberg-dressed atoms

Jorge Mellado Muñoz ¹, Rahul Sawant ^{1,*}, Anna Maffei ^{1,2}, Xi Wang,¹ and Giovanni Barontini ¹

¹*School of Physics and Astronomy, University of Birmingham, Edgbaston, Birmingham B15 2TT, United Kingdom*

²*Dipartimento di Fisica “E. Fermi,” Università di Pisa, Largo B. Pontecorvo 3, 56127 Pisa, Italy*



(Received 29 June 2020; accepted 16 September 2020; published 7 October 2020)

We propose a method to realize the Frenkel-Kontorova model using an array of Rydberg-dressed atoms. Our platform can be used to study this model with a range of realistic interatomic potentials. In particular, we concentrate on two types of interaction potentials: A springlike potential and a repulsive long-range potential. We numerically calculate the phase diagram for such systems and characterize the Aubry-type and commensurate-incommensurate phase transitions. Experimental realizations of this system are also discussed.

DOI: [10.1103/PhysRevA.102.043308](https://doi.org/10.1103/PhysRevA.102.043308)

I. INTRODUCTION

The Frenkel-Kontorova model (FKM) was introduced to describe the structure and the dynamics of a crystal lattice near a dislocation core. It consists of a chain of particles with long-range spring interactions, placed in a sinusoidal potential. Its main characteristic is the competition between the two length scales promoted by these two potentials. Depending on whether the ratio between the interparticle distance and the substrate period is rational or irrational, the particle configuration becomes *commensurate* or *incommensurate* with the substrate. A system in the incommensurate phase can undergo the so-called Aubry phase transition, characterized by the transition from an *unpinned* to a *pinned* configuration when the strength of the substrate potential is increased [1]. This transition is identified by a change in the particle positions and in the phonon spectrum of the ground-state configurations. The FKM has proven useful to describe a multitude of condensed-matter systems. Some examples are the study of dislocation dynamics in solids [2], surfaces and adsorbed atomic layers [3], incommensurate phases in dielectrics [4], crowdions [5], magnetic chains [6], Josephson junctions [7], and tribology [8] using the Frenkel-Kontorova-Tomlinson model [9,10].

Although effective, the FKM uses a nonrealistic infinite-range spring interaction potential. It is therefore beneficial to develop a fully controlled system where the effect of realistic interaction potentials can be tested. Cold-atom systems are ideal candidates for this purpose due to their high degree of control and flexibility. The introduction of optical lattices allowed for the study of several models that explain different condensed-matter phenomena such as the superfluid–Mott insulator phase transition [11,12], Anderson localization [13,14], and the effects of quantum magnetism [15]. Furthermore, long-range interactions can be achieved using atomic species with high permanent dipolar moments [16], dipolar molecules [17], ultracold ions [18], or Rydberg-

dressed atoms [19]. In particular, Rydberg-dressed atoms have the advantage of enabling the control of the range and functional dependence of the interaction potentials, using various Rydberg states for the dressing. These dressed states are achieved by weakly admixing excited Rydberg states with the ground state, using near-resonant light [20] (see Fig. 1).

In this work, we propose the implementation of the FKM with cold Rydberg dressed atoms in an optical lattice. We show that, by using Rydberg dressing and realistic experimental parameters, it is possible to realize at least two different variants of the FKM. As shown in Sec. II, we concentrate in particular on a springlike interaction potential, similar to the original FKM, and a repulsive potential. In Sec. III we calculate the phase diagrams of the system for both cases, which feature the characteristic incommensurate and commensurate configurations. We show how the equilibrium configurations take the form of different *devil's staircases* as the amplitude of the lattice potential is varied. In Sec. IV we concentrate on the system in the incommensurate configuration. We show that, depending of the interaction potential, it is possible to observe either an Aubry-type transition or a crossover from an unpinned phase to a pinned phase. Interestingly, the crossover is characterized by the excitation of a *soft mode*, resembling the phason mode typical of infinite systems. In Sec. V we report our conclusions.

II. SYSTEM

Our system, which is depicted in Fig. 1, consists of N atoms arranged in a one-dimensional (1D) chain placed in a tunable optical lattice, and a dressing field that produces the Rydberg dressed states. We limit the interactions to nearest neighbors since the densities are such that any n -body potential is a sum of two-body potentials.¹ Indicating with x_i and P_i the particle positions and their momenta, the energy of the

*r.v.sawant@bham.ac.uk

¹We checked this explicitly in our case.

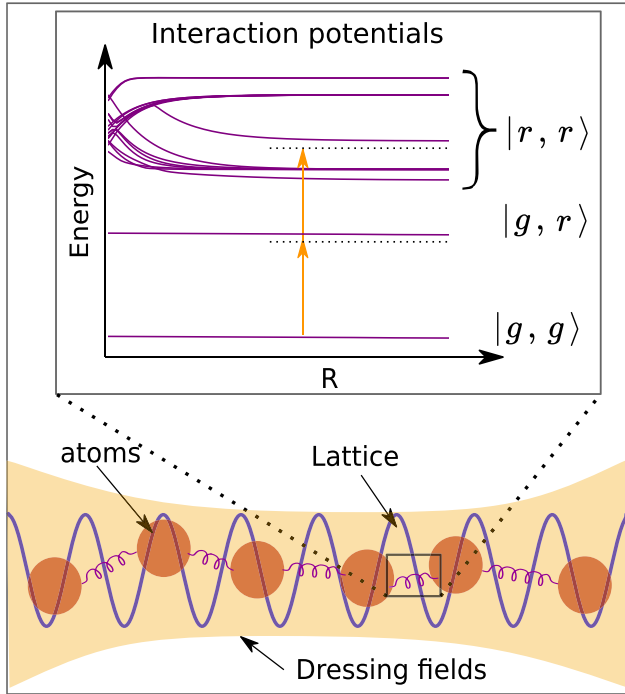


FIG. 1. Schematic of the system for the realization of the Frenkel-Kontorova model. An ensemble of atoms in a 1D optical lattice interacts via Rydberg-dressed potentials. The inset shows how the interatomic potentials can be realized by dressing the atoms' ground state with the Rydberg levels.

system is

$$E = \sum_{i=1}^N \frac{P_i^2}{2m} + \frac{1}{2} \sum_{i=1}^{N-1} c_1 V_{\text{int}}(x_{i+1} - x_i) + \sum_{i=1}^N [V_0 - V_0 \cos(2\pi x_i/b)], \quad (1)$$

where $V_{\text{int}}(x_{i+1} - x_i)$ is the normalized nearest-neighbor interaction between the particles, c_1 is a coefficient that accounts for the amount of Rydberg admixture in the dressed state, V_0 is the depth of the lattice potential, and b is the lattice spacing. m is the mass of the atoms.

We study the system for two different interaction potentials that can be realistically implemented. One is a *springlike* potential and the other a *repulsive* potential, as depicted in Figs. 2(a) and 2(b), respectively. The derivation of these potentials from the Rydberg spectrum is shown in the Appendix A. The functional form of the *springlike* potential is

$$V_{\text{int}} = \frac{-1}{1 + c_0(r - r_0)^2} + \frac{e^{-c_2(r-r'_0)}}{c_1}, \quad (2)$$

where r_0 , c_0 , c_1 , c_2 , and r'_0 are parameters that depend on the details of the Rydberg dressing. The shape of the *repulsive* potential is instead given by

$$V_{\text{int}} = \frac{1}{1 + e^{c_0(r-r_0)}} + \frac{e^{-c_2(r-r'_0)}}{c_1}. \quad (3)$$

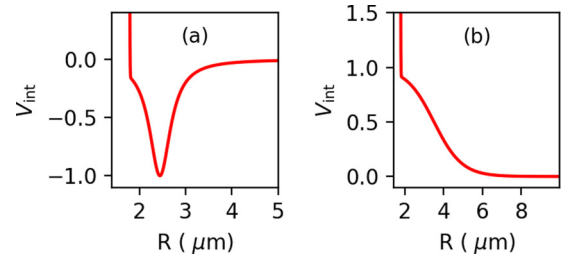


FIG. 2. Normalized interatomic potentials obtained by dressing the atoms with Rydberg states, as explained in the text. (a) The springlike potential. (b) The repulsive potential.

In order to give a specific example, we choose ^{87}Rb atoms dressed with the Rydberg levels $60P_{1/2}$ or $60S_{1/2}$, to realize the two interaction potentials, springlike or repulsive, respectively (details are in the Appendix A). The dressing of the atoms can be realized by a two-photon transition in the case of $60S_{1/2}$, using two lasers at 421.67 and 1013.76 nm for the $5S_{1/2} \rightarrow 6P_{1/2}$ and $6P_{1/2} \rightarrow 60S_{1/2}$ transitions, respectively. While the dressing using $60P_{1/2}$ can be realized by a single-photon transition $5S_{1/2} \rightarrow 60P_{1/2}$, addressed by a 297.11-nm laser. With these parameters we have $r_0 = 3.5 \mu\text{m}$, $c_0 = 1.4 \mu\text{m}^{-1}$, $c_1/k_B = 248.9 \text{ nK}$, $c_2 = 145.0 \mu\text{m}^{-1}$, and $r'_0 = 1.8 \mu\text{m}$ for the repulsive potential and $r_0 = 2.4 \mu\text{m}$, $c_0 = 12.9 \mu\text{m}^{-1}$, $c_1/k_B = 783.6 \text{ nK}$, $c_2 = 263.0 \mu\text{m}^{-1}$, $r'_0 = 1.8 \mu\text{m}$ for the springlike potential.

Concerning the tunable optical lattice, it is possible to realize it by interfering two light beams at an angle. This angle can then be varied to change the lattice spacing [21,22] allowing for lattice periods in the desired range, which in this work we choose to be 1.9–4.5 μm . The system that we propose can be practically implemented. Indeed, Rydberg-dressed atoms have proven to be stable against losses in an optical lattice [23].

III. PHASE DIAGRAMS

In this section, we compute the phase diagram for the ground state of the system for both the dressed potentials. As mentioned above, the FKM is characterized by two length scales, which in our case are the lattice spacing b and the distance a that minimizes V_{int} . The mean interatomic distance \tilde{a} that minimizes E when $V_0 \neq 0$ will, therefore, result from the competition between these two length scales. In particular, depending on which value \tilde{a} takes, the phase diagram breaks between commensurate and incommensurate phases. In a commensurate configuration, the positions of the atoms can be expressed as $x_{Q+i} = x_i + Rb$, where Q and R are integers and i denotes the index of the particle. Therefore, the mean interparticle distance is the rational number $\tilde{a}/b = R/Q$. An incommensurate configuration is instead characterized by an irrational value of \tilde{a}/b .

To compute the ground state and derive the phase diagrams, we use the generalized simulating annealing algorithm [24]. We find the minimum of the energy functional (1) for different values of V_0 and b , with the condition that all the particles are at rest ($P_i = 0$). For both cases, we consider a system of $N = 50$ atoms. In the repulsive case, we add hard walls to

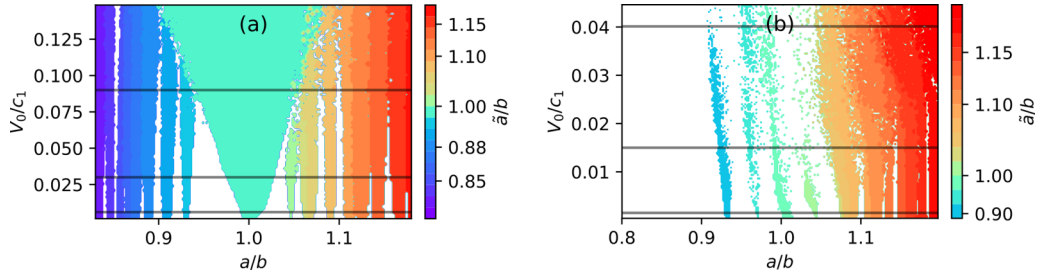


FIG. 3. Phase diagram showing \tilde{a}/b as a function of a/b and V_0/c_1 for (a) the springlike potential and (b) the repulsive potential. Each color represents a different lock-in region, characterized by a commensurate configuration where \tilde{a}/b is rational.

confine the system and prevent the particles from separating indefinitely. Such hard walls could be realized using the technique of reference [25]. We chose the distance between the confining walls so that $a = 3.17 \mu\text{m}$. In the springlike case, a is instead fixed by the minimum of the interaction potential, which in our specific case is at $a = 2.44 \mu\text{m}$.

The resulting phase diagrams are shown in Fig. 3, where we report \tilde{a}/b as a function of a/b and V_0 . In particular, the colored regions indicate the largest *lock-in regions* for \tilde{a}/b , corresponding to commensurate configurations. The white regions are characterized by smaller lock-in regions and incommensurate configurations. In both phase diagrams, for $V_0 = 0$ the system is in the so-called *floating phase* where a/b can take any value. As V_0 is increased, commensurate configurations become more energetically favorable and the phase diagram starts to break into lock-in regions. Indeed, around each rational value of a/b there are intervals in which \tilde{a}/b take the same rational value. The amplitude of the lock-in regions increases as V_0 increases. For the trivial case $V_0/c_1 \gg 1$ all the particles are pinned in the minima of the lattice potential and therefore only commensurate configurations are possible.

Let us first analyze the springlike interaction case, which is the one more similar to the original FKM. In Fig. 4(a) we report \tilde{a}/b as a function of a/b for three values of V_0/c_1 , indicated as black horizontal lines in Fig. 3. As can be seen in Fig. 4(a.1), for small but finite values of V_0/c_1 small intervals of zero slope start to appear in the curve \tilde{a}/b vs a/b . Such intervals are centered around commensurate values of a/b and correspond to \tilde{a}/b taking the same rational value (horizontal dashed lines). As the curve is a combination of zero and nonzero slope regions, it is referred to as an *incomplete devil's staircase*. The lock-in regions exist because the transition from a rational to an irrational value involves the creation of a *discommensuration*, which costs energy. This can be seen in Fig. 4(b.1), where we report the energy per particle as a function of a/b . As a/b moves away from a rational value, the energy per particle starts to increase. When this energy exceeds the energy required to create a discommensuration, a transition to an incommensurate phase occurs. As reported in Figs. 4(a.2) and 4(a.3), when V_0/c_1 is further increased, the width of the lock-in regions increases and incommensurate configurations start to disappear. Eventually, as shown in Fig. 4(a.3), the curve \tilde{a}/b vs a/b becomes a *complete devil's staircase*. The transition from an incomplete to a complete devil's staircase is of special interest for some condensed-matter systems like, e.g., polymers. Also, in this case, moving away from the center of the lock-in region leads to an increase

of the energy per particle, until “jumping” to the next lock-in region becomes energetically favorable.

The same analysis for the repulsive case is reported in Figs. 4(c) and 4(d). In this case, an *anomalous* incomplete devil's staircase is formed in the function \tilde{a}/b vs a/b . The anomaly is in the fact that the lock-in regions are not characterized by a zero slope, and therefore are a mixture of commensurate and incommensurate configurations. This is reflected also in Fig. 3(b), where a large part of the phase diagram is not covered by commensurate configurations. The anomalous lock-in regions increase as V_0 is increased, but the slope remains finite even for large values of V_0 , therefore, the devil's staircase remains always incomplete. Similar to the springlike interaction potential, the lock-in regions are characterized by the increase of the energy per particle as the system moves away from the center of the region.

IV. INCOMMENSURATE CONFIGURATIONS

The competition between the lattice potential and the interatomic potential becomes apparent when the two systems are incommensurate with each other, i.e., when the ratio a/b is highly irrational and quite far from a rational value. In this section, we analyze the behavior of such a system. We first look at how the ground-state configuration of the particle undergoes a phase transition from an unpinned phase to a pinned phase. The pinned phase is characterized by the particles taking only a handful of specific locations with respect to the lattice potential. We then study the phonon spectrum of the ground state and see how the transition changes with the two dressed interaction potentials. In the original FKM, an incommensurate system containing infinite particles can undergo a phase transition called the Aubry phase transition when V_0/c_1 crosses a critical point [26]. This can also be interpreted as a transition from an unpinned phase to a pinned one. Additionally, this type of transition is characterized by the appearance of a gap for the minimum frequency in the phonon spectrum [27]. For our finite system of particles, we observe an analogous Aubry-type transition for the springlike case, while we observe a smooth crossover for the repulsive case.

In Fig. 5 we report $x_i/b \bmod 1$, which gives the particle position with respect to the lattice phase, as a function of V_0/c_1 , for both the dressed potentials. To provide a specific example, we chose the configuration with $a/b = 0.873$. In the trivial case of $V_0/c_1 \approx 0$, the particles are not restricted to any

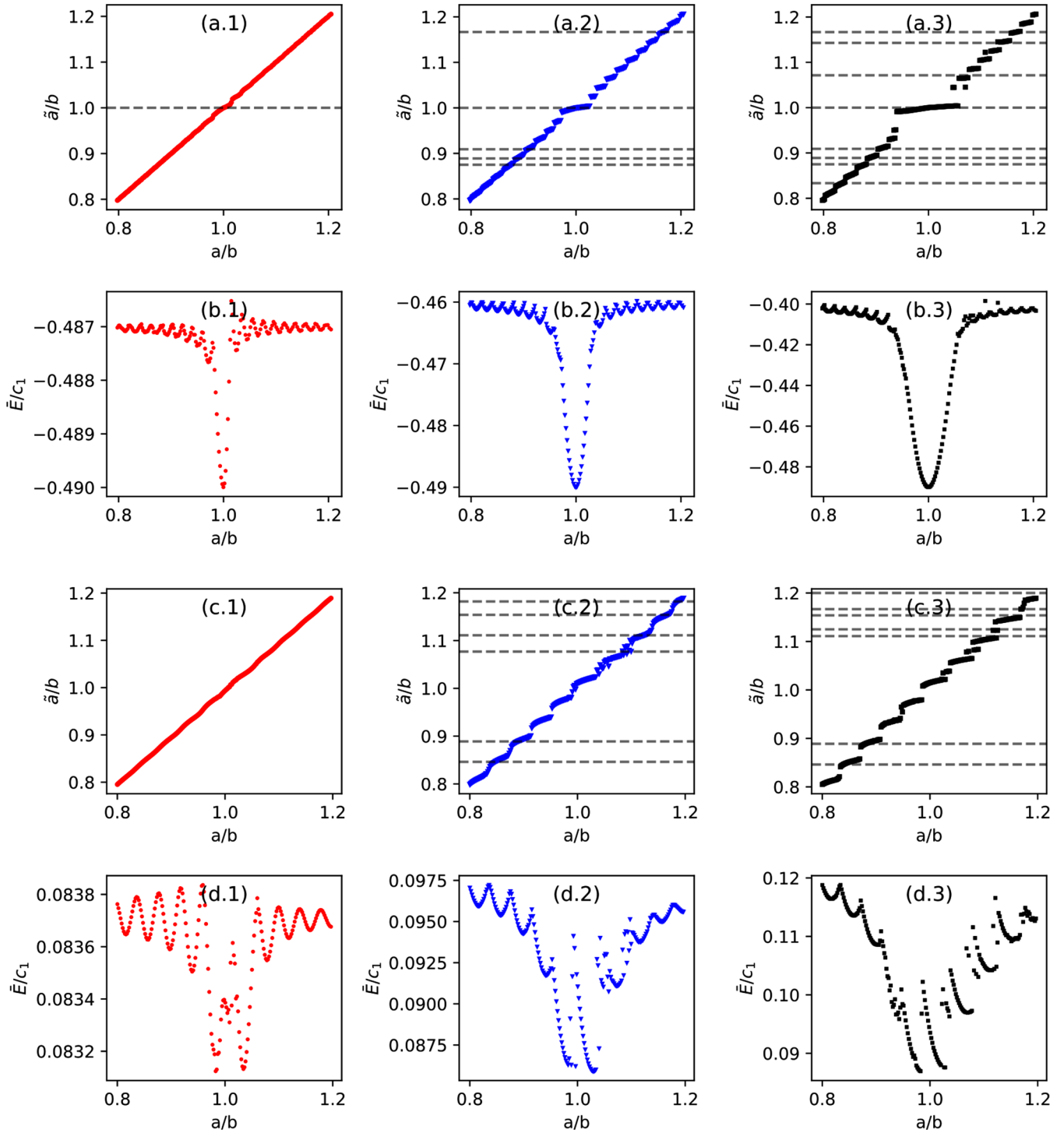


FIG. 4. (a.1)–(a.3) and (c.1)–(c.3) show the mean interparticle distance with respect to the ratio a/b for springlike and repulsive potentials, respectively. (b.1)–(b.3) and (d.1)–(d.3) show the energy per particle (\bar{E}) with respect to the ratio a/b . Here, $V_0/c_1 = 0.006, 0.03, 0.09$ and $0.0015, 0.015, 0.04$ for springlike and repulsive potentials, respectively. The horizontal dashed lines show the locations of a few rational values of \bar{a}/b .

particular position with respect to the lattice. In the springlike case, as V_0 is increased, there is a rather abrupt transition to a configuration where the number of allowed positions is drastically reduced. The system is in the unpinned phase until $V_0/c_1 = 0.19$, after which it undergoes a steep transition to the pinned phase. For the repulsive case, we observe a relatively smoother crossover between $V_0/c_1 = 0.03$ and 0.04

from the unpinned phase to the pinned phase, as can be seen in Fig. 5(b).

Another signature of the transition can be found in the phonon spectrum of the ground-state configurations. An infinite incommensurate system in the unpinned phase presents a gapless Goldstone mode called *phason*. The phason is associated to the invariance of the uniform relative translation

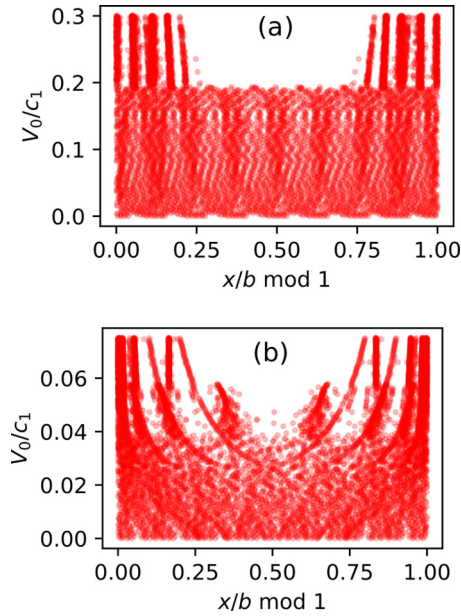


FIG. 5. Particle position with respect to the lattice potential for each value of V_0/c_1 for (a) the springlike and (b) the repulsive case, respectively. Here, the system is incommensurate with the ratio $a/b = 0.873$.

of the phases of modes with relatively irrational periodicities. As the system undergoes the Aubry transition to the pinned phase, this mode disappears. This is a consequence of the pinning of the particles to the substrate, not allowing for the dynamics of this zero-frequency mode. Since our system is finite, such phason mode does not appear in the unpinned phase. However, as we show here below, for the springlike case we observe a similar kind of transition while, for the repulsive case, a *soft mode* appears in correspondence of the crossover from the unpinned to pinned phase. A soft mode is an excitation above the ground state whose energy vanishes in the limit $N \rightarrow \infty$ [28], where it becomes a phason.

We calculate the phonon spectrum of different configurations using the previously calculated ground states and the introduction of the dynamical matrix, defined as

$$D_{kl} = \left. \frac{\partial^2 E}{\partial x_k \partial x_l} \right|_{\{x_i^G\}}, \quad (4)$$

where $D_{k,l}$ are the elements of the dynamical matrix and $\{x_i^G\}$ is the ground-state particle configuration. The eigenvalues of this matrix are λ_j for $j = 1, N$ and they are related to the frequencies of the possible phonon modes ω_j , as $\omega_j^2 = \lambda_j$. For convenience, we introduce the adimensional phonon frequency $\bar{\omega}_j$, defined as $\bar{\omega}_j = \omega_j \sqrt{ma^2/c_1}$ where m is the mass of the particles.

In Figs. 6(a.1) and 6(b.1) we report the frequency of the 15 lowest-energy modes for the springlike and repulsive cases, respectively. The blue dots are for the unpinned phase and the red triangles are for the pinned phase. To provide a specific example, we chose $a/b = 0.873$. For both dressed potentials, the minimum frequency is almost zero below the transition, while the gap becomes larger in the pinned phase. In both cases, we can observe the formation of a staircase in the

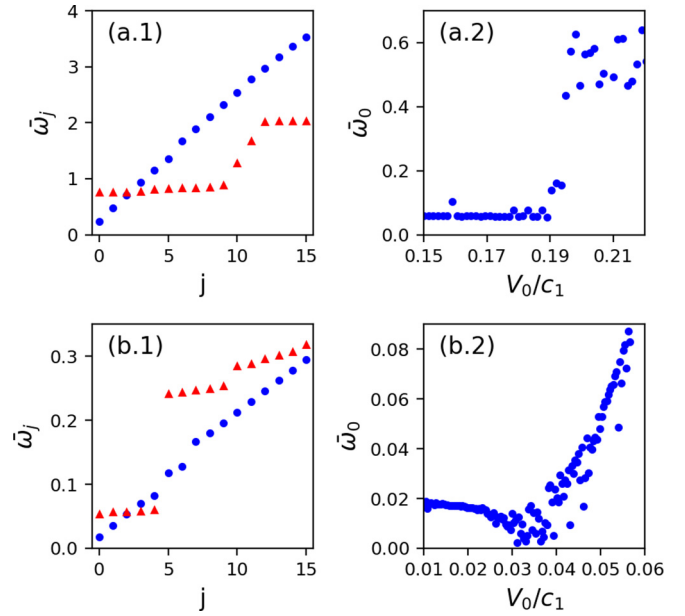


FIG. 6. (a.1) Adimensional frequencies for the 15 lowest modes of the phonon spectrum for the springlike case for $V_0/c_1 = 0.180$ (blue dots) and $V_0/c_1 = 0.201$ (red triangles). (b.1) The same for the repulsive case for $V_0/c_1 = 0.01275$ (blue dots) and $V_0/c_1 = 0.024$ (red triangles). (a.2), (b.2) Show the frequency of the lowest mode as a function of V_0/c_1 . In all cases the system is incommensurate with the ratio $a/b = 0.873$.

phonon spectrum as V_0 is increased. This behavior is similar to the one of the original FKM, in which a staircase formation is also observed in the phonon spectrum in the incommensurate case [27].

In Figs. 6(a.2) and 6(b.2) we report the lowest-energy mode $\bar{\omega}_0$ as a function of V_0/c_1 , for the springlike and repulsive case, respectively. For the springlike case the gap opens up suddenly for $V_0/c_1 \simeq 0.19$, indicating indeed that the system undergoes the Aubry-type transition from the unpinned to the pinned phase, in agreement with Fig. 5(a). For the repulsive case, instead, the energy of $\bar{\omega}_0$ first decreases until it approaches zero for $V_0/c_1 \simeq 0.032$. For this value, the system supports a soft mode, similar to the infinite FKM. As V_0/c_1 is further increased, the energy of $\bar{\omega}_0$ increases again, and the system crosses over to the pinned phase. As a/b moves away from an irrational value and approaches a rational one, both the Aubry-type transition for the springlike case and the crossover for the repulsive case happen for lower values of V_0/c_1 , until a commensurate configuration is reached.

V. CONCLUSIONS

In conclusion, we have proposed a system of Rydberg dressed atoms in an optical lattice as a platform for the study of the FKM with realistic potentials. We have reported the phase diagrams for two dressed potentials that can be realized experimentally. We have shown that, depending on the shape of the interaction potential, the system can exhibit different behaviors. In particular, with a springlike potential, the phenomenology is very close to the original FKM, while for a repulsive potential, the system exhibits

some anomalous features. This is particularly apparent in incommensurate configurations, where the springlike case undergoes an Aubry-type transition as the height of the lattice is increased, while the repulsive case is characterized by a relatively smooth crossover from the unpinned to the pinned phase.

The required Rydberg dressing can be implemented using the details from the Appendix A. In order to find the ground states, a possible experiment could involve cooling the atoms in a lattice, setting the lattice depth to the desired value and then slowly raising the strength of the Rydberg dressing fields to introduce the interatomic potential. This is achievable in current experiments, for example, those in [20,29], where interesting many-body dynamics enabled by Rydberg dressing has been observed. For the specific case described at the end of Sec. II, the phase diagram could be explored with samples at temperatures ranging from a few nK to tens of nK. Such temperatures should be sufficiently low to distinguish between the different locking regions, as reported in Fig. 4. The observables discussed in our work could be extracted in an experiment using established techniques like the quantum gas microscope (see, e.g., [20,29] and references therein). This would allow one to measure the position of each single atom, and therefore evaluate \tilde{a} and $x_i/b \bmod 1$ and reconstruct the phase diagrams.

Producing Rydberg-dressed atoms with lifetimes long enough to observe the FKM physics is a challenging task, due to unwanted off-resonant scattering. It is important to notice that, for the specific case presented, and considering current laser technology, the timescale for the dressing of each atom is limited to ~ 10 ms, because of off-resonant scattering. This can, however, be overcome by quickly repumping to the Rydberg-dressed state, keeping the average number of Rydberg-dressed atoms constant. This effect could be strongly reduced employing higher power lasers that will allow to obtain the targeted level of Rydberg admixture with larger detunings.

Phenomena like ionization by blackbody radiation and avalanche ionization can affect the effective implementation of the proposal. However, these are not fundamental limitations: Blackbody radiation can be strongly suppressed, even using cryogenic systems [30,31], and the very low densities discussed in this work should prevent the onset of avalanche mechanisms like the one discussed in [32].

The proposed system can be extended to other kinds of interaction potentials, including attractive ones, using different dressing schemes. It is relatively straightforward to set up moving optical lattices to implement the Frenkel-Kontorova-Tomlinson model and perform tribology studies with unprecedented control. This will allow one to access the spectrum reported in Fig. 6, in particular, it would be interesting to probe the onset of the soft modes, for which the underlying optical lattice should slide almost without friction. Previous implementations of this system with cold ions have proven both theoretically [33,34] and experimentally [18,35–37] that cold-atom systems are an excellent platform to study nanofriction and other phenomena related to the properties of the FKM. Another extremely interesting direction could be to extend the system in two dimensions, where numerical calculations are difficult, and where an experimental implementation could provide new insight.

ACKNOWLEDGMENTS

The authors are supported by the Leverhulme Trust Research Project Grant UltraQuTe (Grant No. RGP-2018-266). A.M. is supported by the Erasmus programme.

J.M.M. and R.S. contributed equally to this work.

APPENDIX A: RYDBERG DRESSING

In this Appendix, we will discuss how we get the Rydberg-dressed potentials we use in this work. To first order, the interaction between Rydberg-dressed atoms can be easily calculated assuming a simple dipole-dipole interaction between atoms excited to Rydberg levels. In Ref. [38], the authors calculated the potential between Rydberg-dressed atoms using such an approximation and only considering a single Rydberg level. In practice, as the Rydberg levels are closely spaced, multiple Rydberg levels have to be considered. Additionally, the dipole-dipole interaction studied in Ref. [38] requires an electric field. The potentials derived in this work are, however, for the zero electric field case. Importantly, in our analysis, we consider multiple Rydberg levels.

In general, the Hamiltonian for two atoms interacting with a light field nearly resonant with a Rydberg level can be written as

$$\begin{aligned}
 H(t) = \hbar & \left[\sum_i \omega_i (|g, r_i\rangle \langle g, r_i| + |r_i, g\rangle \langle r_i, g|) + \sum_{i,j} (\omega_i + \omega_j) (|r_j, r_i\rangle \langle r_j, r_i| + |r_i, r_j\rangle \langle r_i, r_j|) \right. \\
 & + \sum_i 2\Omega_i e^{-i\omega_i t} (|g, g\rangle \langle g, r_i| + |g, g\rangle \langle r_i, g|) + 2\Omega_i^* e^{i\omega_i t} (|g, r_i\rangle \langle g, g| + |r_i, g\rangle \langle g, g|) \\
 & + \sum_{i,j} 2\Omega_i e^{-i\omega_i t} (|g, r_j\rangle \langle r_i, r_j| + |r_j, g\rangle \langle r_j, r_i|) + 2\Omega_i^* e^{i\omega_i t} (|r_i, r_j\rangle \langle g, r_i| + |r_j, r_i\rangle \langle r_i, g|) \\
 & \left. + \sum_{i,j,k,l} D_{ijkl}(R) |r_i, r_j\rangle \langle r_k, r_l| + D_{ijkl}^*(R) |r_k, r_l\rangle \langle r_i, r_j| \right]. \tag{A1}
 \end{aligned}$$

Here, the state $|g, r_i\rangle$ denotes that the first atom is its ground state ($|g\rangle$) and the second atom is in the i th Rydberg state ($|r_i\rangle$). $\hbar\omega_i$ is the energy of the i th Rydberg state with respect to the ground state, $\omega_L/(2\pi)$ is the frequency of the dressing laser, $\Omega_i/(2\pi)$

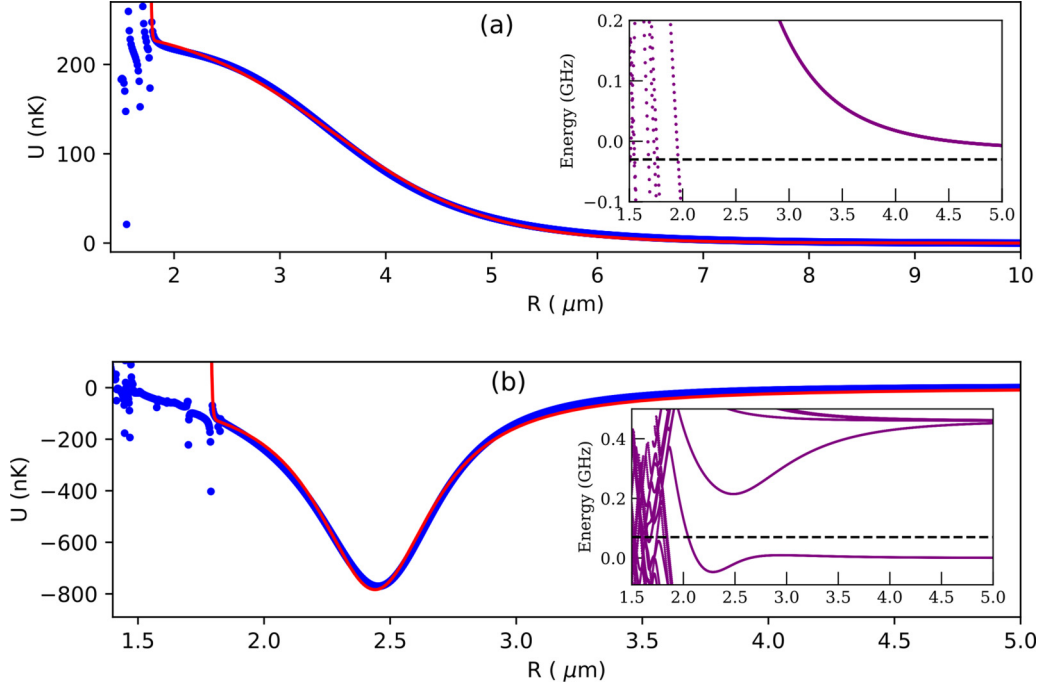


FIG. 7. Top panel. (a) The energy of the state dressed by $60S_{1/2}$ Rydberg level for ^{87}Rb atoms as a function of interatomic distance. Here $\Omega_t/2\pi = 8$ MHz and $\Delta_t/2\pi = 30$ MHz. The fit (red line) function is $248.9/(1 + e^{1.382(x-3.494)}) + e^{-145(x-1.811)}$. For the numerical diagonalization, 243 Rydberg states were used, and the Rydberg-Rydberg interaction included dipole-dipole, quadrupole-dipole, and quadrupole-quadrupole terms. Inset shows how the interaction between Rydberg atoms changes as a function of interatomic distance. The dressed line shows where the dressed laser is resonant. Lower panel. (b) The energy of the state dressed by $60P_{1/2}$ Rydberg level for ^{87}Rb atoms as a function of interatomic distance. Here $\Omega_t/2\pi = 15$ MHz and $\Delta_t/2\pi = -70$ MHz. The fit function is $783.6/[1 + 12.95(x - 2.44)^2] + e^{-263(x-1.813)}$. For the numerical diagonalization, 282 Rydberg states were used, and the Rydberg-Rydberg interaction included dipole-dipole, quadrupole-dipole, and quadrupole-quadrupole terms. Inset shows how the interaction between Rydberg atoms changes as a function of interatomic distance. The dressed line shows where the dressed laser is resonant.

is the Rabi frequency induced by the dressing laser for the transition $|g\rangle \rightarrow |r_i\rangle$, and $D_{ijkl}(R)$ is the interaction between Rydberg level pairs (r_i, r_j) and (r_k, r_l) as a function of interatomic distance R .

We can go to a rotating frame of reference using the following unitary transformation:

$$U(t) = |g, g\rangle \langle g, g| + \sum_i e^{-i\omega_L t} (|g, r_i\rangle \langle g, r_i| + |r_i, g\rangle \langle r_i, g|) + \sum_{ij} e^{-2i\omega_L t} (|r_i, r_j\rangle \langle r_i, r_j| + |r_j, r_i\rangle \langle r_j, r_i|). \quad (\text{A2})$$

The Hamiltonian in this rotating frame becomes

$$\begin{aligned} H_r &= U(t)H(t)U^\dagger(t) + i\hbar U(t) dU^\dagger(t)/dt \\ &= \hbar \left[\sum_i \Delta_i (|g, r_i\rangle \langle g, r_i| + |r_i, g\rangle \langle r_i, g|) + \sum_{i,j} (\Delta_i + \Delta_j) (|r_j, r_i\rangle \langle r_j, r_i| + |r_i, r_j\rangle \langle r_i, r_j|) \right. \\ &\quad + \sum_i 2\Omega_i (|g, g\rangle \langle g, r_i| + |g, g\rangle \langle r_i, g|) + 2\Omega_i^* (|g, r_i\rangle \langle g, g| + |r_i, g\rangle \langle g, g|) \\ &\quad + \sum_{i,j} 2\Omega_i (|g, r_j\rangle \langle r_i, r_j| + |r_j, g\rangle \langle r_j, r_i|) + 2\Omega_i^* (|r_i, r_j\rangle \langle g, r_i| + |r_j, r_i\rangle \langle r_i, g|) \\ &\quad \left. + \sum_{i,j,k,l} D_{ijkl}(R) |r_i, r_j\rangle \langle r_k, r_l| + D_{ijkl}^*(R) |r_k, r_l\rangle \langle r_i, r_j| \right], \quad (\text{A3}) \end{aligned}$$

where $\Delta_i = \omega_i - \omega_L$ is the detuning of the laser from the transition formed by $|g\rangle$ and $|r_i\rangle$. We are interested in coupling the laser light to a single Rydberg state r_t , where t denotes the target state. To do this we choose a laser wavelength such that $\Delta_i \gg \Delta_r$ for all $i \neq t$. In this case we can neglect all levels $|g, r_{i \neq t}\rangle$ and $|r_{i \neq t}, g\rangle$ as such states will not be excited. We keep the levels $|r_i, r_j\rangle$ as $D_{ijkl}(R)$ is of the same order of magnitude as Δ_t and that is where the R dependence will come from. In such a scenario, the

Hamiltonian reduces to

$$\begin{aligned}
 H_r = \hbar \left[\Delta_t(|g, r_i\rangle \langle g, r_i| + |r_i, g\rangle \langle r_i, g|) + \sum_{i,j} (\Delta_i + \Delta_j)(|r_j, r_i\rangle \langle r_j, r_i| + |r_i, r_j\rangle \langle r_i, r_j|) \right. \\
 + 2\Omega_i(|g, g\rangle \langle g, r_i| + |g, g\rangle \langle r_i, g|) + 2\Omega_i^*(|g, r_i\rangle \langle g, g| + |r_i, g\rangle \langle g, g|) \\
 + \sum_i 2\Omega_i(|g, r_i\rangle \langle r_i, r_i| + |r_i, g\rangle \langle r_i, r_i|) + 2\Omega_i^*(|r_i, r_i\rangle \langle g, r_i| + |r_i, r_i\rangle \langle r_i, g|) \\
 \left. + \sum_{i,j,k,l} D_{ijkl}(R) |r_i, r_j\rangle \langle r_k, r_l| + D_{ijkl}^*(R) |r_k, r_l\rangle \langle r_i, r_j| \right]. \tag{A4}
 \end{aligned}$$

We numerically diagonalize the above Hamiltonian to get the dressed eigenstate and extract the eigenvalue closest to the state $|g, g\rangle$. For an atom dressed primarily with the $60S_{1/2}$ Rydberg state of ^{87}Rb atom, the lowest eigenvalue as a function of the interatomic distance is shown in

Fig. 7(a). Similarly, if the dressing laser is tuned near the $60P_{1/2}$ Rydberg level, we get a dressed potential as shown in Fig. 7(b).

For the numerical diagonalization, we modified the Python library named ARC [39] to include the dressing field.

-
- [1] O. M. Braun and Y. S. Kivshar, *The Frenkel-Kontorova Model: Concepts, Methods, and Applications* (Springer, New York, 2013).
 - [2] E. Fitzgerald, Dislocations in strained-layer epitaxy: Theory, experiment, and applications, *Mater. Sci. Rep.* **7**, 87 (1991).
 - [3] O. Braun and V. Medvedev, Interaction between particles adsorbed on metal surfaces, *Sov. Phys. Usp.* **32**, 328 (1989).
 - [4] R. Blinc and A. Levanyuk, *Incommensurate Phases in Dielectrics* (North-Holland, Amsterdam, 1986), Vol. 1.
 - [5] W. Xiao, P. A. Greaney, and D. C. Chrzan, Adatom Transport on Strained CU (001): Surface Crowdions, *Phys. Rev. Lett.* **90**, 156102 (2003).
 - [6] R. A. Cowley, J. D. Axe, and M. Iizumi, Neutron Scattering from the Ferroelectric Fluctuations and Domain Walls of Lead Germanate, *Phys. Rev. Lett.* **36**, 806 (1976).
 - [7] D. W. McLaughlin and A. C. Scott, Perturbation analysis of fluxon dynamics, *Phys. Rev. A* **18**, 1652 (1978).
 - [8] A. Vanossi, N. Manini, M. Urbakh, S. Zapperi, and E. Tosatti, Colloquium: Modeling friction: From nanoscale to mesoscale, *Rev. Mod. Phys.* **85**, 529 (2013).
 - [9] M. Weiss and F.-J. Elmer, Dry friction in the Frenkel-Kontorova-Tomlinson model: Static properties, *Phys. Rev. B* **53**, 7539 (1996).
 - [10] M. Weiss and F.-J. Elmer, Dry friction in the frenkel-kontorova-tomlinson model: Dynamical properties, *Z. Phys. B: Condens. Matter* **104**, 55 (1997).
 - [11] D. Jaksch, C. Bruder, J. I. Cirac, C. W. Gardiner, and P. Zoller, Cold Bosonic Atoms in Optical Lattices, *Phys. Rev. Lett.* **81**, 3108 (1998).
 - [12] M. Greiner, O. Mandel, T. Esslinger, T. W. Hänsch, and I. Bloch, Quantum phase transition from a superfluid to a mott insulator in a gas of ultracold atoms, *Nature (London)* **415**, 39 (2002).
 - [13] G. Roati, C. D’Errico, L. Fallani, M. Fattori, C. Fort, M. Zaccanti, G. Modugno, M. Modugno, and M. Inguscio, Anderson localization of a non-interacting bose-einstein condensate, *Nature (London)* **453**, 895 (2008).
 - [14] J. Billy, V. Josse, Z. Zuo, A. Bernard, B. Hambrecht, P. Lugan, D. Clément, L. Sanchez-Palencia, P. Bouyer, and A. Aspect, Direct observation of anderson localization of matter waves in a controlled disorder, *Nature (London)* **453**, 891 (2008).
 - [15] D. Greif, T. Uehlinger, G. Jotzu, L. Tarruell, and T. Esslinger, Short-range quantum magnetism of ultracold fermions in an optical lattice, *Science* **340**, 1307 (2013).
 - [16] M. Lu, N. Q. Burdick, S. H. Youn, and B. L. Lev, Strongly Dipolar Bose-Einstein Condensate of Dysprosium, *Phys. Rev. Lett.* **107**, 190401 (2011).
 - [17] J. A. Blackmore, L. Caldwell, P. D. Gregory, E. M. Bridge, R. Sawant, J. Aldegunde, J. Mur-Petit, D. Jaksch, J. M. Hutson, B. Sauer *et al.*, Ultracold molecules for quantum simulation: Rotational coherences in caf and rbc, *Quantum Sci. Technol.* **4**, 014010 (2018).
 - [18] A. Bylinskii, D. Gangloff, and V. Vuletić, Tuning friction atom-by-atom in an ion-crystal simulator, *Science* **348**, 1115 (2015).
 - [19] G. Pupillo, A. Micheli, M. Boninsegni, I. Lesanovsky, and P. Zoller, Strongly Correlated Gases of Rydberg-Dressed Atoms: Quantum and Classical Dynamics, *Phys. Rev. Lett.* **104**, 223002 (2010).
 - [20] J. Zeiher, R. Van Bijnen, P. Schauß, S. Hild, J.-y. Choi, T. Pohl, I. Bloch, and C. Gross, Many-body interferometry of a rydberg-dressed spin lattice, *Nat. Phys.* **12**, 1095 (2016).
 - [21] T. C. Li, H. Kelkar, D. Medellin, and M. G. Raizen, Real-time control of the periodicity of a standing wave: An optical accordion, *Opt. Express* **16**, 5465 (2008).
 - [22] J. L. Ville, T. Bienaimé, R. Saint-Jalm, L. Corman, M. Aidelburger, L. Chomaz, K. Kleinlein, D. Perconte, S. Nascimbène, J. Dalibard, and J. Beugnon, Loading and compression of a single two-dimensional bose gas in an optical accordion, *Phys. Rev. A* **95**, 013632 (2017).
 - [23] T. Macrì and T. Pohl, Rydberg dressing of atoms in optical lattices, *Phys. Rev. A* **89**, 011402(R) (2014).
 - [24] C. Tsallis and D. A. Stariolo, Generalized simulated annealing, *Phys. A (Amsterdam)* **233**, 395 (1996).

- [25] A. L. Gaunt, T. F. Schmidutz, I. Gotlibovych, R. P. Smith, and Z. Hadzibabic, Bose-Einstein Condensation of Atoms in a Uniform Potential, *Phys. Rev. Lett.* **110**, 200406 (2013).
- [26] S. Aubry, The twist map, the extended frenkel-kontorova model and the devil's staircase, *Phys. D (Amsterdam)* **7**, 240 (1983).
- [27] L. M. Floría and J. J. Mazo, Dissipative dynamics of the frenkel-kontorova model, *Adv. Phys.* **45**, 505 (1996).
- [28] S. R. Sharma, B. Bergersen, and B. Joos, Aubry transition in a finite modulated chain, *Phys. Rev. B* **29**, 6335 (1984).
- [29] J. Zeiher, J.-y. Choi, A. Rubio-Abadal, T. Pohl, R. van Bijnen, I. Bloch, and C. Gross, Coherent Many-Body Spin Dynamics in a Long-Range Interacting Ising Chain, *Phys. Rev. X* **7**, 041063 (2017).
- [30] R. C. Teixeira, C. Hermann-Avigliano, T. L. Nguyen, T. Cantat-Moltrecht, J. M. Raimond, S. Haroche, S. Gleyzes, and M. Brune, Microwaves Probe Dipole Blockade and van der Waals Forces in a Cold Rydberg Gas, *Phys. Rev. Lett.* **115**, 013001 (2015).
- [31] C. Hermann-Avigliano, R. C. Teixeira, T. L. Nguyen, T. Cantat-Moltrecht, G. Nogues, I. Dotsenko, S. Gleyzes, J. M. Raimond, S. Haroche, and M. Brune, Long coherence times for rydberg qubits on a superconducting atom chip, *Phys. Rev. A* **90**, 040502(R) (2014).
- [32] E. A. Goldschmidt, T. Boulier, R. C. Brown, S. B. Koller, J. T. Young, A. V. Gorshkov, S. L. Rolston, and J. V. Porto, Anomalous Broadening in Driven Dissipative Rydberg Systems, *Phys. Rev. Lett.* **116**, 113001 (2016).
- [33] A. Benassi, A. Vanossi, and E. Tosatti, Nanofriction in cold ion traps, *Nat. Commun.* **2**, 1 (2011).
- [34] T. Pruttivarasin, M. Ramm, I. Talukdar, A. Kreuter, and H. Häffner, Trapped ions in optical lattices for probing oscillator chain models, *New J. Phys.* **13**, 075012 (2011).
- [35] A. Bylinskii, D. Gangloff, I. Counts, and V. Vuletić, Observation of aubry-type transition in finite atom chains via friction, *Nat. Mater.* **15**, 717 (2016).
- [36] J. Kiethe, R. Nigmatullin, D. Kalincev, T. Schmirander, and T. Mehlstäubler, Probing nanofriction and aubry-type signatures in a finite self-organized system, *Nat. Commun.* **8**, 1 (2017).
- [37] D. A. Gangloff, A. Bylinskii, and V. Vuletić, Kinks and nanofriction: Structural phases in few-atom chains, *Phys. Rev. Res.* **2**, 013380 (2020).
- [38] J. E. Johnson and S. L. Rolston, Interactions between rydberg-dressed atoms, *Phys. Rev. A* **82**, 033412 (2010).
- [39] N. Šibalić, J. D. Pritchard, C. S. Adams, and K. J. Weatherill, Arc: An open-source library for calculating properties of alkali rydberg atoms, *Comput. Phys. Commun.* **220**, 319 (2017).